

Article

The Sediments in the Beibu Gulf Reveal Dramatic Paleoenvironmental Changes and Climate Events over the Past ~20,000 Years

Yuchun Li ¹, Tianlai Fan ^{1,*}, Aihua Wang ^{2,3}, Jun Zeng ^{4,5}, Yubiao Lv ^{4,5}, Mingwang Zhang ¹ and Dajun Liu ¹

¹ Guangxi Laboratory on the Study of Coral Reefs in the South China Sea, Coral Reef Research Center of China, School of Marine Sciences, Guangxi University, Nanning 530004, China; 15941454960@163.com (Y.L.); zmw0612@163.com (M.Z.); gxu_ldj@163.com (D.L.)

² Nanjing Hongchuang Exploration Technology Service, Nanjing 210023, China; jsnjywa@163.com

³ Nanjing Center, China Geological Survey, Nanjing 210016, China

⁴ Guangxi Academy of Sciences, Nanning 530007, China; gdyelhbkj@163.com (J.Z.); lyuyubiao@163.com (Y.L.)

⁵ Institute of Beibu Gulf Marine Industry, Fangchenggang 538000, China

* Correspondence: fantl2004@hotmail.com

Abstract: The geochemical characteristics of a 2.1 m BBW25 core, collected from the Beibu Gulf, have been investigated in terms of the major and trace elements, organic matter, and CaCO_3 and AMS ^{14}C dating by XRF, ICP-OES, ICP-MS, and more. We have found through previous research that there are issues with unclear delineation of sedimentary evolution environments and inexact responses between chemical weathering intensity and major paleoclimate events in the Beibu Gulf. The AMS ^{14}C dating results indicate that the sedimentary age at the bottom was 19.24 ky b.p. CaCO_3 , $\delta^{13}\text{C}$, C/N, and Sr/Ba indexes show a sedimentary environment change from terrestrial to marine environments and a “jump” of ~4000 years in continent–ocean changes. The evolution of the sedimentary environment of Beibu Gulf was divided into three environments and five sub-environments. The changes in chemical weathering intensity indicators recorded by the CIX and the Fe/Al ratio respond well to the East Asian monsoon cycle, the meltwater events, and the alternation of cold and warm events. This study explains the chemical weathering intensity and sedimentary environment in the BBW25 core by geochemical characteristics and further reveals the paleoenvironmental characteristics and possible driving mechanisms over the past ~20,000 years.

Keywords: Beibu Gulf; core sediment; geochemical characteristics; sedimentary environment; climate change



Citation: Li, Y.; Fan, T.; Wang, A.; Zeng, J.; Lv, Y.; Zhang, M.; Liu, D. The Sediments in the Beibu Gulf Reveal Dramatic Paleoenvironmental Changes and Climate Events over the Past ~20,000 Years. *J. Mar. Sci. Eng.* **2024**, *12*, 615. <https://doi.org/10.3390/jmse12040615>

Academic Editor: Gemma Aiello

Received: 27 February 2024

Revised: 26 March 2024

Accepted: 27 March 2024

Published: 2 April 2024



Copyright: © 2024 by the authors. Licensee MDPI, Basel, Switzerland. This article is an open access article distributed under the terms and conditions of the Creative Commons Attribution (CC BY) license (<https://creativecommons.org/licenses/by/4.0/>).

1. Introduction

As part of the South China Sea, the largest marginal sea in the western Pacific, the Beibu Gulf preserved information on changes in the marine environment with sediments since the late last glacial maximum (LGM), and its deposition processes are highly impacted by land-sea interactions, sea-level changes, East Asian monsoons (EAMs), and other processes. The Beibu Gulf, located on the northwestern edge of the South China Sea, is a semi-enclosed bay with an area of approximately $12.93 \times 10^4 \text{ km}^2$, an average depth of 42 m, and a maximum depth of 100 m. It is located in the shelf area of the South China Sea and is connected to this sea through the Qiongzhou Strait. Due to its unique geographical location, diverse seabed topography, and complex ocean currents and hydrodynamic environment, its marine sediments preserve rich paleoclimatic information in East Asia [1–11].

Since the end of the last glacial maximum (LGM) (20,000 years before the present), the climate system of the Beibu Gulf has experienced the Heinrich1 (H1) cold, Bølling-Allerød (BA) warm, Meltwater Pulse 1B (MWP-1B), Younger Dryas (YD) cold, and Holocene rhythmic cooling (Bond) events. Prior studies have extensively investigated the geochemical

characteristics of these sediments and provided important information on sea level, sea surface temperature (SST), and circulation changes; sediment source-to-sink processes; as well as chemical weathering intensity changes and coastal erosion processes in the surrounding continents. The acquisition of knowledge regarding the interactions between paleoclimate and continent–ocean changes is crucial for the comparative analysis and comprehensive understanding of present and future interconnections among these systems. Currently, there are disagreements regarding the delineation of sedimentary evolution environments and responses between the chemical weathering intensity and major paleoclimate events in the Beibu Gulf [12–19].

The C4 and B106 cores in the central and southern parts of the Beibu Gulf indicated that the Beibu Gulf was a terrestrial to marine–terrestrial alternating sedimentary environment prior to 13.4 ka BP. The STAT22 core indicated a marine–terrestrial alternating sedimentary environment at around 11.1 ka BP. The inconsistent paleoclimatic events in different latitude regions may reflect the lagging response of low-latitude regions to the global climate or the existence of regional special climate change mechanisms. In fact, in the South China Sea, there are differences in the Paleoclimatic events revealed by data from different cores, and even different research methods used at the same core can yield different results, possibly due to limitations in certain methods or environmental constraints. The TWS-1, ZK20, ZK001, and PC338 cores in the South China Sea indicated that the chemical weathering intensity in the northwest of the South China Sea was significantly higher in the Holocene than in the glacial stage, while the KT2 core indicated an opposite conclusion [20–26].

Through a review of previous research, it was found that the classification of sedimentary environments in the Beibu Gulf mainly focused on the Holocene or the late last deglaciation, without considering the early last deglaciation or the LGM. Simultaneously, the indicators for chemical weathering intensity and sedimentary environments have remained largely unchanged, and the new indicators developed in recent years have not been introduced. Therefore, this study discusses changes in the marine environment of the Beibu Gulf and high-resolution information on possible climate responses through investigating geochemical characteristics in the core sediments. Thus, our work aims at improving our understanding of the changes in the marine environment of marginal seas over the past 20,000 years and their correlation with global climate change.

2. Material and Methods

2.1. Materials

As shown in Figure 1, sampling point BBW25 is located in the offshore area southwest of Hainan Island ($108^{\circ}08.9166' E$, $18^{\circ}07.2945' N$). A gravity piston sampler was used to sample the columnar core sediment, with an overlying water depth of 84 m and an overall length of approximately 2.1 m. The samples had high viscosity and exhibited a homogeneous fluid–soft plastic mud state. Occasionally, bivalve and gastropod debris could be seen in the upper part. The lithology was mainly clay with a small amount of fine sand. The lower sediment contained almost no shell debris and was composed of clay (Figure 1). The core samples were stored in a freezer (below $-20^{\circ}C$) in the cabin laboratory of the ship and then transferred to Guangdong Ocean University for cryopreservation. To avoid the effects of benthic disturbance, resuspension, and seafloor re-sedimentation, the core was cut into 210 samples (1 cm per sample). All samples were wrapped with pre-sanitized aluminum foil and sealed in sterile polyethylene bags. One quarter of each sample was taken for subsequent experiments in this study.

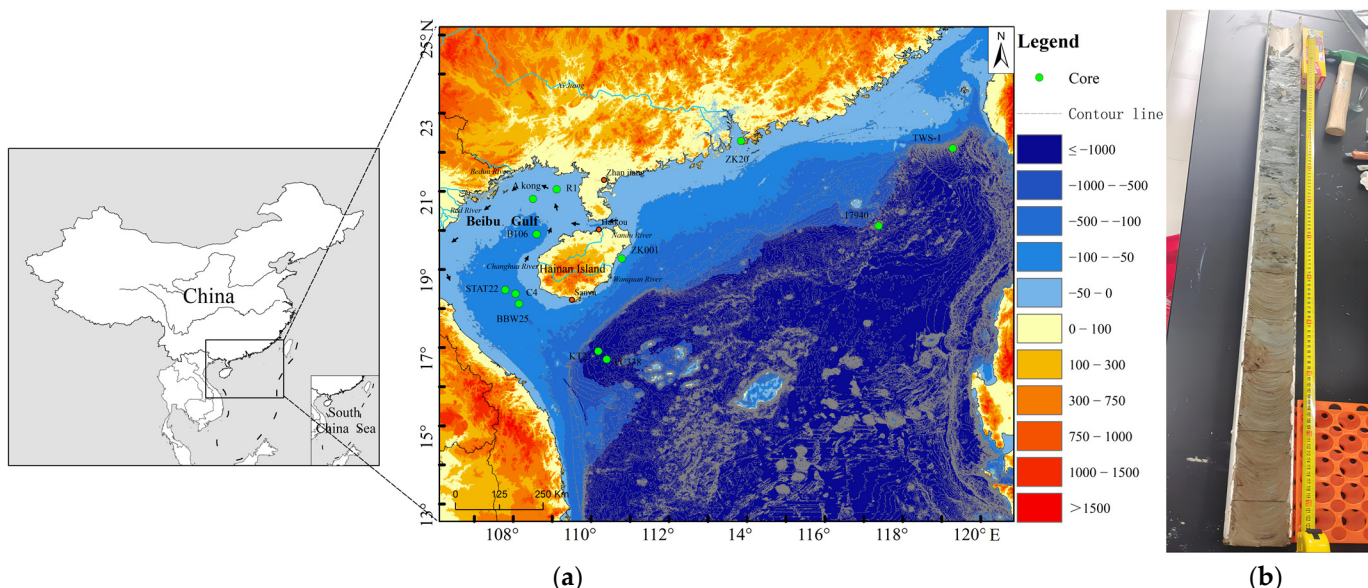


Figure 1. BBW25 sediment core: (a) Topographic map of core BBW25 sampling location, surrounding areas, and the cores mentioned in the article; (b) core profile.

2.2. Methods

The samples were first placed in an oven at 60 °C for drying and then ground to below 200 mesh. Rock powder samples were sent to BETA Laboratory for AMS ^{14}C dating. The sample type was organic sediment, and the pre-treatment method was acid washing. The half-life of ^{14}C used for dating was 5568 years. The calibration program was BetaCal4.20, the calibration method was the HPD method, and the database used was MARINE20. Measured ages were corrected by ^{13}C fractionation to obtain conventional ages, and the conventional ages were corrected by the tree ring to obtain calendar ages. To facilitate the calculation, interval averages with high confidence (2σ , 95.4%) of the corrected ages were mainly used in the comparison of AMS ^{14}C ages. The corrected calendar ages were calculated on this basis. Chemical element contents of rock powder samples were measured using a (NITON XL3T) handheld X-ray fluorescence spectrometer (XRF—School of Marine Sciences, Guangxi University, Nanning, China). Major element contents of the processed samples were detected using (HORIBA) inductively coupled plasma optical emission spectroscopy (ICP-OES—Nanjing Hongchuang Exploration Technology Service Co. Ltd., Nanjing, China) and the processing and experimental processes were referred to Chemical analysis methods of silicate rocks Part 31: Determination of 12 components such as silica [27]. The rock powder samples were washed with 10% hydrochloric acid (Qingtian Biotechnology Co. Ltd., Nanning, China) for 24 h. The solid residues were rinsed with deionized water, centrifuged eight times for a neutral pH, and dried at 60 °C. After acid washing, TOC and TN contents of the rock powder samples were detected using the (vario MACRO cube) element analyzer (School of Marine Sciences, Guangxi University, Nanning, China). After acid washing, the samples were mixed with rod-shaped copper oxide and platinum wire as catalysts, then burnt at 800–850 °C in the experimental furnace with O_2 introduced. The generated CO_2 was released after condensation and purification in a liquid nitrogen cold trap for detection of organic carbon isotope ($\delta^{13}\text{C}_{\text{V-PDB}}$). $\delta^{13}\text{C}_{\text{V-PDB}}$ contents of the rock powder samples were detected using the (Vario EL III/Isoprime) elemental analyzer-isotope ratio mass spectrometer (EA-IRMS—Instrumental Analysis Center of Shanghai Jiao Tong University, Shanghai, China). The content of Sr and Ba selected extraction from the core was detected using (Agilent 7900) Inductively Coupled Plasma Mass Spectrometry (ICP-MS—Nanjing Hongchuang Exploration Technology Service Co. Ltd., Nanjing, China), while the processing and experimental procedures were referred to Chemical Analysis Methods of Silicate Rocks Part 30: Determination of 44 [28,29].

3. Results

3.1. Construction of the Stratigraphic Age and Sedimentation Rate Frameworks Based on AMS ^{14}C

Samples were taken for AMS ^{14}C testing at depths of 40, 75, 120, 160, and 210 cm in the core. These results are represented by “cal. ka BP”, which means “calibrated thousand years before present”, abbreviated as “ka BP”. The age framework should be established based on these results, and the Bayesian age-depth model should be utilized to acquire more comprehensive and precise age information of the BBW25 sediment core [30]. The sedimentation rate of the upper profile is 0.008 cm/yr, and the lower profile is 0.102 cm/yr.

According to Figure 2 and Table 1, the age at the bottom of the sedimentary column in borehole BBW25 is 19.24 ka BP. In the sections above and below the burial depth of 119–120 cm, the age of the sediments changes significantly. The sedimentation rates of the upper and lower sections also have obvious changes, which can be attributed to changes in climate, sea level, or the source of the sediments [11].

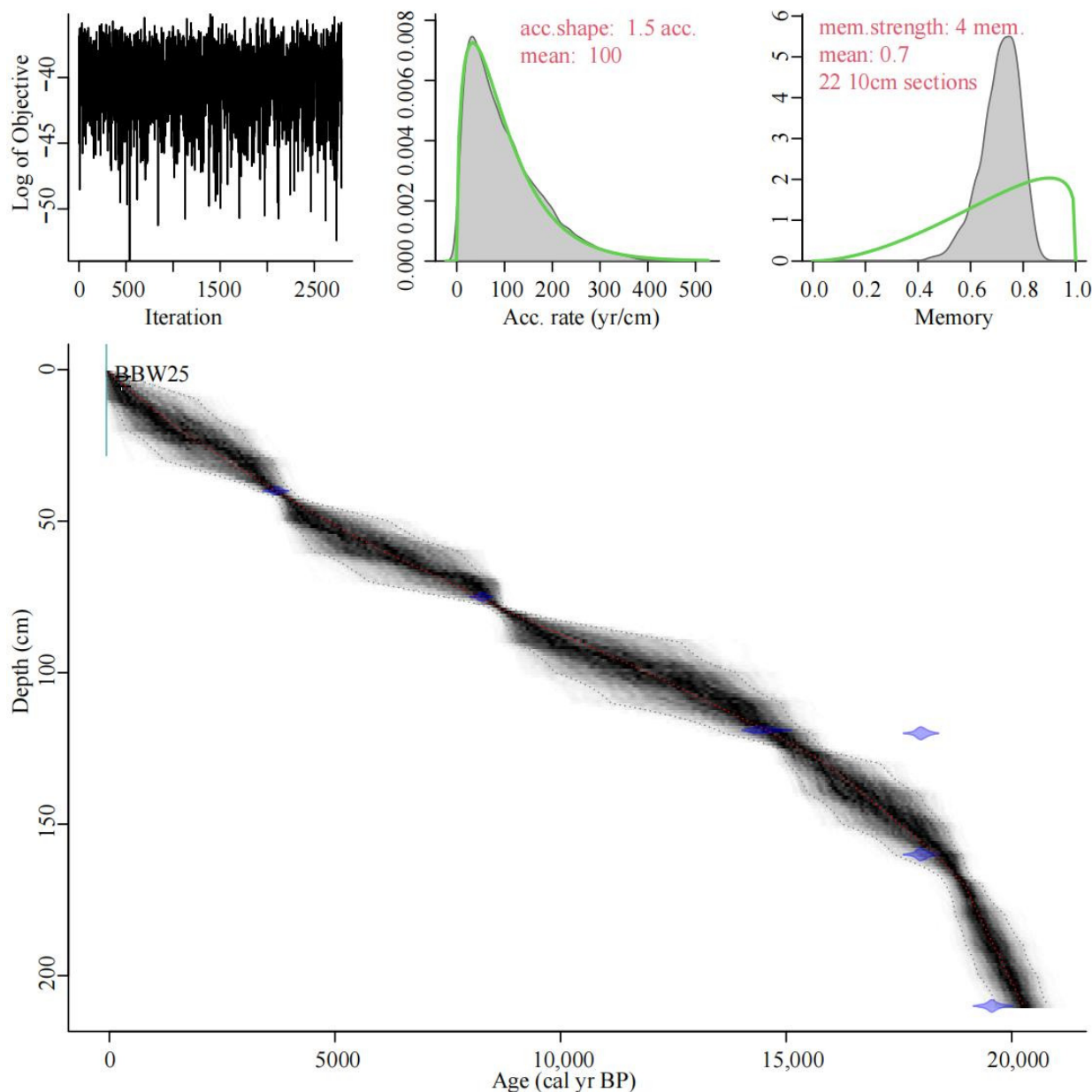


Figure 2. Bayesian age-depth model.

Table 1. BBW25 core AMS ^{14}C age results.

Depth (cm)	Conventional Radiocarbon Age	Age Correction (95.4% Probability)	Calibrated Average Calendar Age
40	3850 ± 30 BP	(72.5%) 2456–2271 cal BC 4405–4220 cal BP (22.9%) 2260–2204 cal BC 4209–4153 cal BP (95.4%)	4281 BP
75	7880 ± 30 BP	6368–6068 cal BC 8317–8017 cal BP (95.4%)	8167 BP
119	$12,890 \pm 40$ BP	12,891–12,299 cal BC 14,840–14,248 cal BP (95.4%)	14,544 BP
120	$15,850 \pm 50$ BP	16,648–16,180 cal BC 18,597–18,129 cal BP (53%) 16,545–16,354 cal BC 18,494–18,303 cal BP	18,363 BP
160	$15,290 \pm 50$ BP	16,803–16,649 cal BC 18,752–18,598 cal BP (95.4%)	18,521 BP
210	$16,700 \pm 50$ BP	17,542–17,047 cal BC 19,491–18,996 cal BP	19,244 BP

3.2. Changes in Major Elements

Contents of major elements in core sediments also show a similar age-depth model pattern to that in the upper and lower profiles. Contents of major elements vary with the burial depth as shown in Figure 3. Among them, CaO and MgO contents exhibited patterns similar to those in the upper and lower sections in the age framework. The average content is ranked as $\text{SiO}_2 > \text{Al}_2\text{O}_3 > \text{Fe}_2\text{O}_3 > \text{CaO} > \text{K}_2\text{O} > \text{Na}_2\text{O} > \text{TiO}_2 > \text{P}_2\text{O}_5$. Among them, the SiO_2 content range is 50–70%; Al_2O_3 content is 8–15%; Fe_2O_3 content is 3–7%; CaO content is 0.2–8.5%; K_2O and MgO content is 1–4%; Na_2O content is 0.9–1.3%; TiO_2 content is 0.6–1.1%; P_2O_5 content is 0.09–0.2%; and MnO content is 0.02–0.07%. Figure 3a shows the results of the ICP-MS tests, which were performed at 10 cm intervals, for a total of 20 samples tested. Figure 3b shows the results of the XRF tests, which were performed at 1 cm intervals, for a total of 210 samples tested.

3.3. Changes in Organic Matter

Organic matter proxies and the content of Sr and Ba in the core sediments also show a similar age-depth model pattern to that in upper and lower sections. The variation in organic matter content with burial depth is shown in Figure 4, with a similar pattern of upper and lower sections in the age framework. The TOC content range of core sediment was 0.28–0.71%; TN content was 0.03–0.12%; and $\delta^{13}\text{C}_{\text{V-PDB}}$ (hereafter abbreviated as $\delta^{13}\text{C}$) content ranged between -25.5 and $-18.54\text{\textperthousand}$. Organic matter was tested at 2 cm intervals and a total of 105 samples were tested. The Sr content range of core sediment was 7–238.8%; and Ba content was 1.5–18.63%. Sr and Ba were tested at 5 cm intervals and a total of 42 samples were tested.

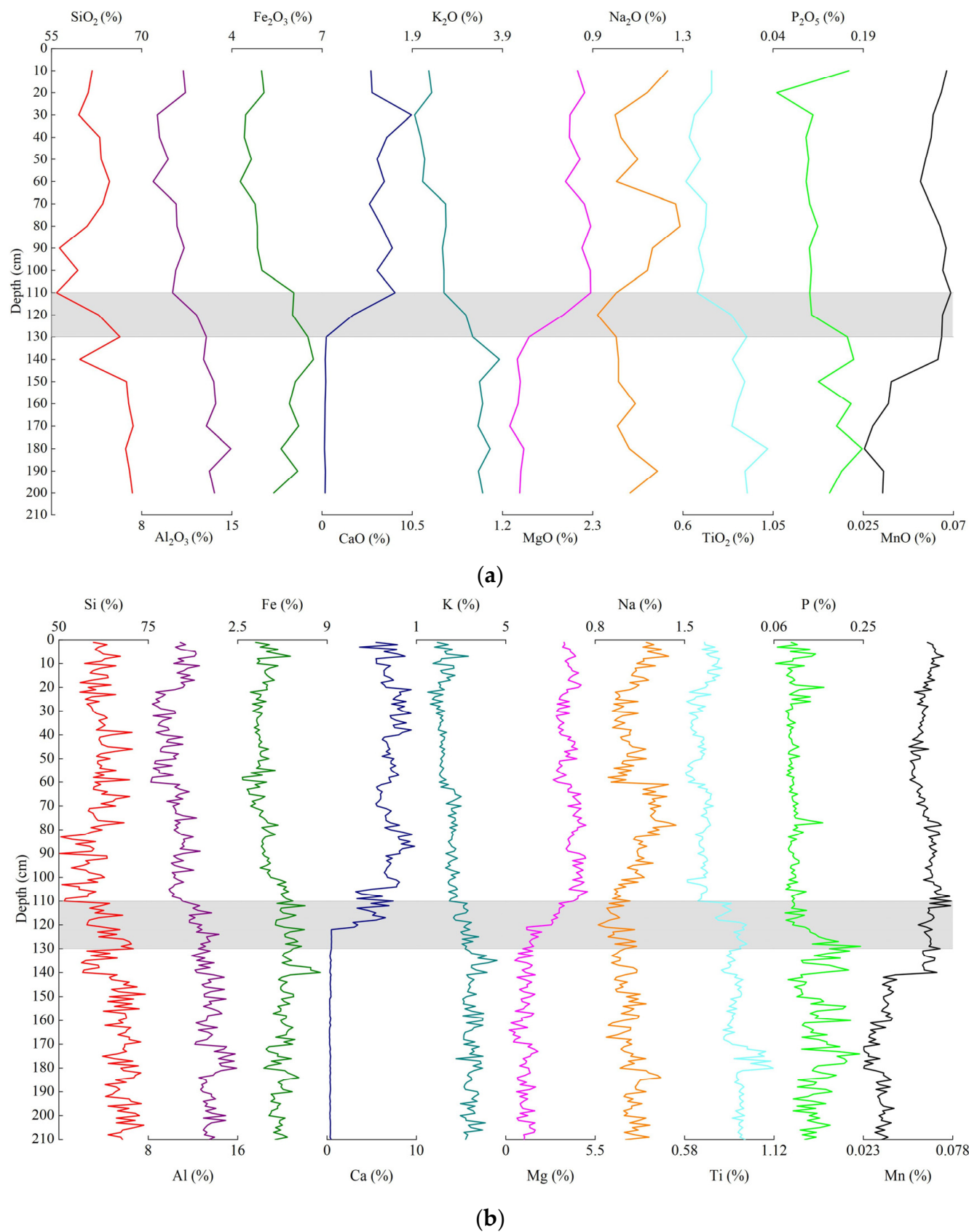


Figure 3. Measurement of major element contents in the BBW25 core: (a) ICP-OES; (b) XRF.

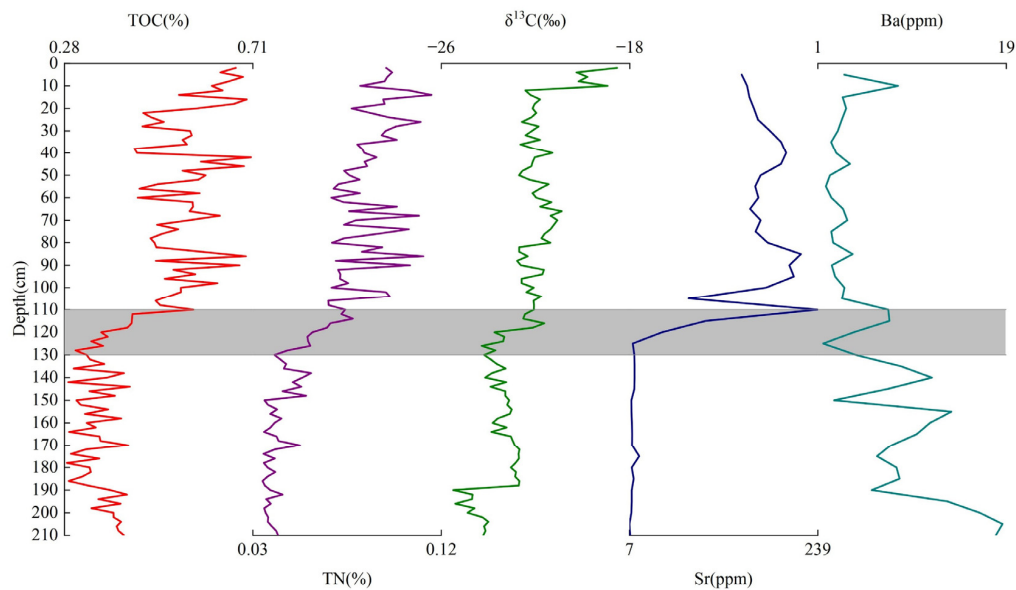


Figure 4. Organic matter proxies and the content of Sr and Ba in the BBW25 core.

3.4. Changes in Carbonate Contents

The carbonate content in the core sediment also shows a similar age-depth model pattern to that of the upper and lower sections. The variation in carbonate content with depth is shown in Figure 5. During the hydrochloric acid dissolution process of the organic matter pretreatment in core sediment, the mass of escaped CO₂ can be derived by calculating the change in sample mass before and after the hydrochloric acid dissolution. Through calculating the mass of emitted CO₂, we can calculate the percentage of CO₃²⁻ and CaCO₃ in the sample. The variation trends of the three groups of data are relatively similar when comparing the CO₃²⁻ content with the CaO and Ca contents measured by ICP-MS and XRF, respectively. Thus, it can be concluded that carbonate mostly existed in the form of calcium carbonate in the sediment. Due to significant errors, the XRF test results had to be corrected. Figure 5 shows that the Ca contents in sediments were relatively high with significant changes. Thus, the relative error can be ignored. Also, Figure 5 indicates that the XRF and ICP-MS test results have consistent changes, proving a good correspondence between the results. Therefore, in this study, the ICP-MS test result data are used to calibrate XRF test result data.

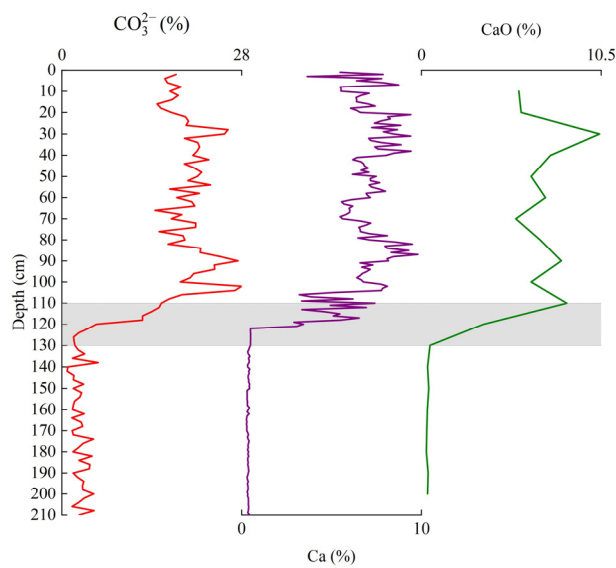


Figure 5. Comparison of carbonate and Ca contents in the BBW25 core.

4. Discussion

4.1. Response of Sedimentary Environments in the Beibu Gulf to Sea Level and Sea Surface Temperature (SST) in the South China Sea over the Past 20,000 years

4.1.1. Changes in Sea Level and SST and the Sedimentary Environment Indicators

As shown in Figure 6, previous studies have obtained information about the relative change in sea level in the South China Sea based on sea level changes in the Sunda shelf, Malacca Strait, and Red River Delta, as well as SST changes in the South China Sea based on changes in long-chain alkenones and $U^{k_{37}}$ in the 17940 core profile [9,31]. Sea level in the South China Sea was positively correlated with the mean SST. As temperatures increased, the ice age ended and glacial melting caused the sea level to rise. As shown in Figure 6, the sea level during the LGM in the South China Sea was estimated to be at least 110 m below its current position, resulting in complete exposure of the Beibu Gulf as terrestrial land. Subsequently, throughout the last deglaciation period, there was a gradual rise in sea level that led to the submergence of previously exposed land, transforming the sedimentary environment of the Beibu Gulf from terrestrial to marine. The BBW25 core sedimentary column was buried at a depth of approximately 84 m in modern times. At approximately 14.6–14.3 ka BP, the sea level was approximately between −87.5 and −82 m when the depth of the BBW25 core sedimentary column was 119–120 cm (depositional age about 14.54 ka BP). This was the location of significant changes in most geochemical characteristic indicators.

The Sr–Ba ratio is a geochemical indicator of paleosalinity in sediments and has been used to indicate the changes and evolution environments of transgression in the Beibu Gulf [22,32,33]. Previous studies in deltaic environments have found that Sr/Ba is <1 in freshwater (rivers), <1–3 in brackish water (delta front), <3–8 in saline water (prodelta), and >8 in normal seawater (shallow sea environment and residual sand) [34,35]. The C/N ratio and $\delta^{13}\text{C}$ are important indicators for determining the source of organic matter in sediments. Based on the ratio of total organic carbon and nitrogen contents in sediments, distinguishing between terrestrial and marine organic matter is possible. Generally, aquatic algae are rich in proteins and lipids, and their organic matter has a lower C/N ratio. Terrestrial higher plants are rich in their carbon content such as cellulose and lignin, while proteins comprise less than 20%. Their organic matter has a higher C/N ratio [36]. Previous studies on the TOC and TN of sediments in various sedimentary environments have found that the C/N ratio of marine sediments ranges between 4–7, while in terrestrial sediments it is ≥ 12 . The C/N ratios for high-salinity and subtidal sediments are about 11.6 and 9.3, respectively. The C/N ratio of mixed marine and terrestrial sediments ranges between 8–12 [37–39]. Based on the C/N changes observed in the borehole in this study, the C/N ratios of 4–8 in the BBW25 core indicates marine sedimentation, while values >8 indicate marine–terrestrial alternating sedimentation. Previous studies on the $\delta^{13}\text{C}$ of sediments in a large number of different sedimentary environments revealed that the $\delta^{13}\text{C}$ of freshwater algae and terrestrial end-members was in the range of −25–−30‰; the $\delta^{13}\text{C}$ of marine algae and seawater end-members was in the range of −16–−23‰; and the $\delta^{13}\text{C}$ of sediments at the bottom of the ocean was in the range of −18–−24‰ [36,37,40–42]. Based on the $\delta^{13}\text{C}$ of BBW25 core sediments in this study, $\delta^{13}\text{C}$ of −18–−23‰ indicated a marine sedimentary environment, $\delta^{13}\text{C}$ of −23–−24‰ indicated a marine–terrestrial alternating sedimentary environment, and $\delta^{13}\text{C}$ of −24–−26‰ indicated a terrestrial sedimentary environment. The BBW25 core is mainly composed of clay particles, with no drastic changes in particle size. Previous studies on minerals in the Beibu Gulf have shown that when hydrodynamic forces are strong, kaolin tends to be present [43]. However, the kaolin content in the upper section of the core is higher than that in the lower section, and there is no kaolin in the lower section, indicating that the upper part of the core is in a marine sedimentary environment. The tectonic subsidence over the past 20,000 years has mainly been concentrated in the Qiongzhou Strait because the Beibu Gulf was a mainly terrestrial environment during the last glacial period, and the Qiongzhou Strait was mainly developed from 11 to 7 ka BP [11,44,45], while the drastic changes in geochemical characteristics of the BBW25 core

occurred at about 14 ka BP. Thus, the changes in the sedimentary environment reflected by the geochemical characteristics of core sediments in the Beibu Gulf can be attributed to the rise in sea level observed in the South China Sea. Figure 5's research indicates that calcium existed in sediments in the form of calcium carbonate. Calcium carbonate can reflect the proportion of biogenic sources in sediments and can be used as a representative for marine inputs. Low contents were associated with an increased transfer of debris from the surrounding continent, while high contents were associated with increased inputs of marine biogenic sources [46].

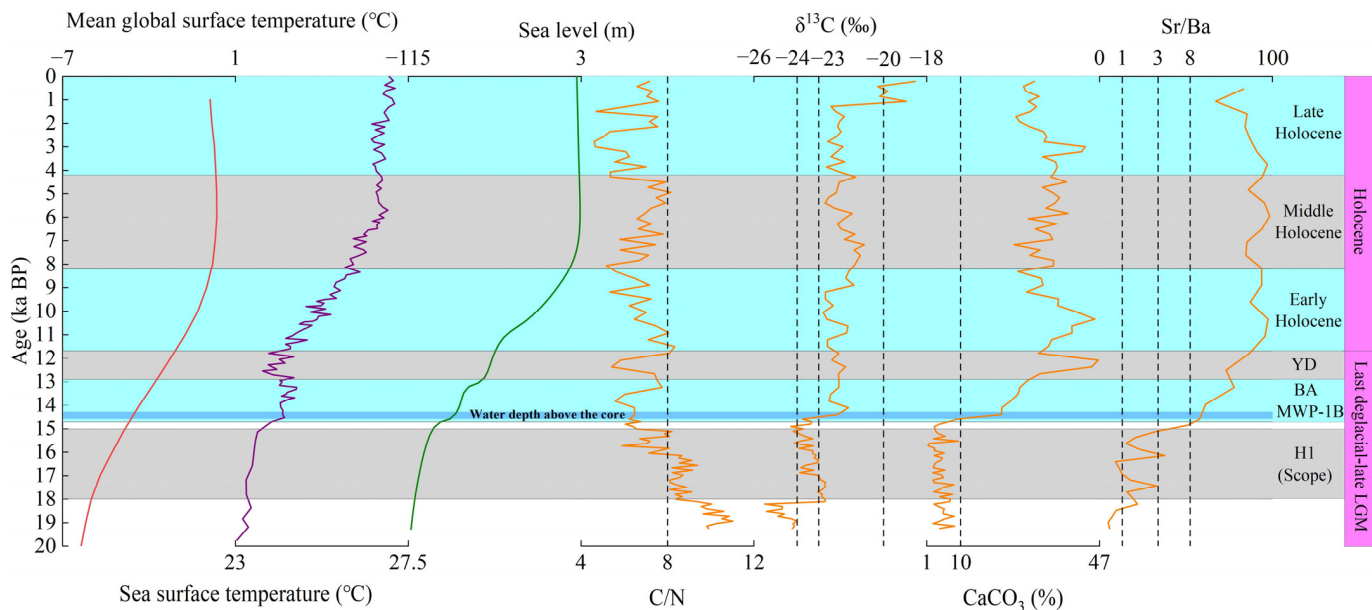


Figure 6. Comparison of sedimentary environment indicators in core over time with mean global surface temperature [47], sea surface temperature [9], and sea level change [31] in the South China Sea.

4.1.2. Establishment of a “Simplified Age-Depth Framework” and Phasing of Sedimentary Evolution

Table 1 shows that there is a “jump” in the age of the sediments at the depth of 119–120 cm, ~4000 years, making classifying sedimentary environments and analyzing chemical weathering intensity in the age-depth framework difficult. This phenomenon also occurred in the STAT22 core (both the STAT22 and BBW25 cores were located in the southern part of the Beibu Gulf). The ages at the burial depths of 290–295 cm and 305–310 cm in the STAT22 core were 11.11 and 17.99 ka BP, respectively, with an age “jump” of ~7000 years for two samples at consecutive burial depths. However, this phenomenon has not been explained. The classification of sedimentary environments in the Beibu Gulf based on the STAT22 core study also began from the Holocene [22]. Our study analyzed the sedimentation rates of seafloor sediments at the depths of 119–120, 160, and 210 cm, as well as the range of sedimentary environment indicators among the depths (sedimentary environment indicators) (Table 1 and Figure 7). It was found that the sedimentation rate of the 150–160 cm core section was 0.253 cm/yr, while the that of the 160–190 cm core section in the same sedimentary environment was 0.069 cm/yr. The sedimentation rates of the two depths differed significantly, which could be due to the mixing of new and old sediments during the last deglaciation, resulting in inaccurate age test results. Previous researchers who studied cores in the South China Sea proposed the theory of “tropical shelf weathering during the ice age” [26]. It was found that during the last ice age, the temperature drop in low-latitude tropical regions was relatively small, resulting in a decrease in sea level and widespread exposure of the continental shelf. Under the combined actions of suitable temperature and humidity, strong groundwater circulation, sufficient reaction time, and a large mineral surface area, the overlying loose deposits

underwent further chemical weathering. At the same time, new land emerged during the LGM. The shelf sediments, which were previously deposited at high sea levels during the interglacial period, may have been re-weathered and transported by river erosion to the river basins near the northwest slope of the South China Sea. Starting from the deglaciation, the sea level rise caused a reduction in the exposed area of the continental shelf. The northwest of the South China Sea received more initial weathering products from river basins through ocean current suspension transport [24,25,48]. Studies on the R1 core near the Weizhou Island in the Beibu Gulf of the South China Sea found that fossils in the late Pleistocene strata (buried at a depth of about 1.5 m) contained Holocene marine sediments and transgression records [49].

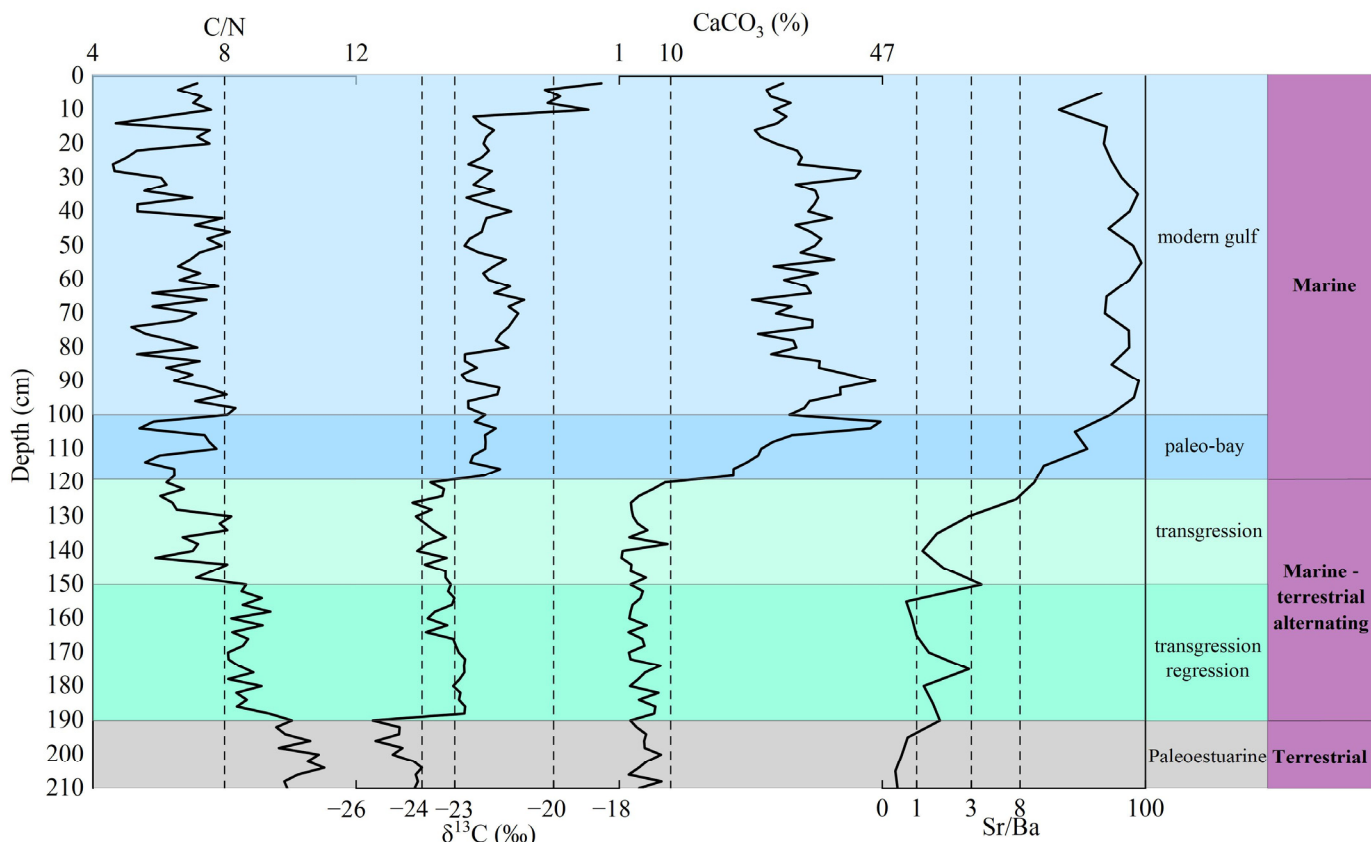


Figure 7. Trend of selected proxies with depth and paleoenvironmental restoration.

In summary, the sediment source timelines in the Beibu Gulf during the last deglaciation were complex. To facilitate the analysis of core sedimentary records, only the carbon-14 age data at burial depths of 119–210 cm was used to establish the “simplified age-depth framework” for the lower section of the core.

Based on the “jump” in calcium carbonate content, combined with the phased variation characteristics of C/N, Sr/Ba, and $\delta^{13}\text{C}$ (Figures 6 and 7), the evolution of the sedimentary environment in the Beibu Gulf was divided into the following three sedimentary environments and five sedimentary sub-environments:

(1) Terrestrial sedimentary environment—paleo-estuarine sub-environment (from 210 to 190 cm) (19.24–18.21 ka BP): This period corresponds to the end of the LGM and the beginning of the last deglaciation. The SST and sea level of the South China Sea did not exhibit a significant increase. During this period, the sea level in the South China Sea was observed to be lower than the current maximum water depth in the Beibu Gulf [50]. In the BBW25 core, from the burial depth of 190 cm to the bottom, the C/N ratio was relatively high; $\delta^{13}\text{C}$ was $<-24\text{\textperthousand}$ and $\delta^{13}\text{C}$ at the bottom of the core was $<-25\text{\textperthousand}$. This indicated that the organic matter input was mainly represented by freshwater plants or terrestrial

particulate matter. The Sr/Ba ratios were all <1 , indicating that sedimentation originated from terrestrial environments. The ratios jointly indicated terrestrial deposits below 190 cm in the BBW25 core.

(2) Marine–terrestrial alternating sedimentary environment—transgression and regression sub-environment (from 190 to 150 cm) (18.21–16.15 ka BP): During this period, the SST and sea level in the South China Sea slowly rose, with seawater possibly entering the Beibu Gulf. At the burial depths of 190–150 cm in the core, the C/N ratio decreased compared to that in the terrestrial environment. At a ratio of 8–9, there was a decreasing and then increasing trend, which may record a transgression and regression. Sr/Ba and $\delta^{13}\text{C}$ showed that at burial depths of 190–166 cm, Sr/Ba was 1–3, which indicates brackish conditions. $\delta^{13}\text{C}$ was between -22 and $-23\text{\textperthousand}$, which corresponds to the seawater end-member organic matter input, indicating a transgression process at that time. Subsequently, at the burial depth of 150 cm, $\delta^{13}\text{C}$ decreased to between -23 and $-24\text{\textperthousand}$. There were both marine and terrestrial organic matter inputs. The decrease of $\text{Sr/Ba} < 1$ indicates a transition to terrestrial sedimentation, and a regression event was recorded. The age of this regression event was relatively consistent with the recorded age of the H1 cold event, which may be due to an impact of the H1 cold event on sea level.

(3) Marine–terrestrial alternating sedimentary environment—transgression sub-environment (from 150 to 119 cm) (16.15–14.54 ka BP): During this period, the SST and sea level in the South China Sea rose rapidly. The sea level rose from -103 m to approximately -86 m. The seawater entered from the mouth of the Nanbu Gulf, arriving at the current BBW25 at a depth of 84 m. The sedimentary record coincided with the sea level. In general, the trends of C/N and calcium carbonate in sediments were opposite [50]. As the sea level rose and seawater invaded the land, the carbonate content increased, and the C/N ratio decreased to below eight. This indicated that the growth of marine calcareous organisms was beginning to flourish, and the dilution effect of terrestrial debris may be weakened [51], leading to an increase in the carbonate content, while the terrestrial contribution of organic matter continued to decrease. $\Delta^{13}\text{C}$ was in the range of -23 – $-24\text{\textperthousand}$, and Sr/Ba was in the range of 1–8, suggesting a continuous environment of transgression.

(4) Marine sedimentary environment—paleo-bay sub-environment (from 119 to 100 cm) (14.54–11.7 ka BP): This period was the beginning of the BA warm event and the end of the YD cold event as well as the occurrence of the MWP-1B event. The South China Sea's SST remained in a fluctuating state without significant increase, influenced by the alternation of warm and cold events. However, under the influence of the MWP-1B event [52], the sea level of South China Sea rose rapidly, from -86 m to approximately -56 m. In this core section, $\delta^{13}\text{C}$ organic matter rose above $-23\text{\textperthousand}$. The C/N ratio decreased, while the Sr/Ba ratio increased rapidly. All these proxies together indicated a clear shift towards marine environmental conditions. Subsequently, seawater continued to invade northward through narrow waterways, affecting the nearshore sedimentation in the Beibu Gulf.

(5) Marine sedimentation environment—modern gulf sub-environment (from 100 to 0 cm) (11.7–1.07 ka BP—present-day): The Holocene epoch witnessed a stabilization of both sea surface temperature (SST) and sea level in the South China Sea, following their earlier rise around 5.5 ka and 8 ka, respectively. It was not until approximately 8.5 ka BP that Hainan Island became completely detached from the Leizhou Peninsula, thereby connecting the Beibu Gulf to the South China Sea through the Qiongzhou Strait. During the early-to-middle Holocene (10–8.5 ka BP and 7–5 ka BP), SST variations were primarily influenced by the East Asian monsoon [53–57]. This phenomenon can also account for the significant fluctuations observed in the sedimentary environmental record indicators within the BBW25 core during the early and middle Holocene. The intensification of monsoon activity resulted in enhanced circulation within the Beibu Gulf, exacerbating terrestrial erosion processes and, consequently, amplifying dilution effects. Therefore, more terrestrial and marine materials were mixed into the sediment. As shown in Figure 6, drastic fluctuations were observed in the sedimentary environment record indicators at burial depths of 100–10 cm (11.7–1.07 ka BP) in the core. But they were all within the range

of marine sedimentary fluctuations, indicating the formation of the modern ocean. $\delta^{13}\text{C}$ rose above $-20\text{\textperthousand}$ at burial depths of 10–0 cm (1.07 ka BP–present-day), suggesting the direct input of organic matter to surface sediments by seawater. This indicates that the modern marine environment in the Beibu Gulf was formed around 1000 years ago.

Previous studies on the thickness of Kong core in the Beibu Gulf found that the depth of marine sediments in the Holocene were located above 1 m; the depth of marine-terrestrial transitional sediments were from 1 to 1.4 m; and the depth of terrestrial stratum sediments were from 1.4 to 2.7 m during the late Pleistocene. The Holocene transgression layer was thinner than the late Pleistocene sedimentary layer [58,59], which was consistent with the thickness recorded in the BBW25 core. The division of sedimentary environments in the Beibu Gulf by previous researchers was different from that of this study. After analyzing the total Sr/Ba and sporopollen in the STAT22 core, it was believed that the paleo-estuarine sub-environment in the Beibu Gulf was between 11.1 and 9 ka BP, the period of expansion from the paleo-estuarine sub-environment to the paleo-bay sub-environment and maintaining stability was 9–6–4 ka BP, and the period of the modern gulf sub-environment and maintaining stability was from 4–1 ka BP–the present-day. The comprehensive analysis of pollen, spores, and algae in the C4 and B106 cores suggested that the Beibu Gulf was in a terrestrial to marine-terrestrial alternating sub-environment before 13.4 ka BP; a paleo-bay sub-environment from 13.4 to 11.7 ka BP; and a modern marine sub-environment from 11.7 ka BP to the present day [9,21].

4.2. Response of the Intensity of Terrestrial Weathering in the Potential Source Area to Climate Events in East Asia over the Past 20,000 Years

Previous studies have demonstrated that chemical weathering can alter the elemental composition of sediments, both in terms of major and trace elements. These changes are primarily influenced by climate variations. The process of element migration within sediment source areas has the potential to reverse climate change patterns and provide insights into paleoclimate reconstruction. Geochemical characteristics and ratios of sedimentary elements serve as commonly employed indicators for quantifying the intensity of chemical weathering. Therefore, it is crucial to carefully select effective element tracers for assessing chemical weathering intensity and reconstructing paleoclimate events [60–63].

4.2.1. Source Area Analysis of Core Sediments

By comparing the findings from previous studies on the sediment source-to-sink process in the northwest South China Sea (Figure 8) with the core location examined in this study, it is inferred that the BBW25 core sediment originates from the Red River, Pearl River (including Qinjiang river within its water system), and Hainan Island. Previous research has indicated that the chemical weathering of sediments in these areas is influenced by the East Asian monsoon, exhibiting a similar intensity trend to monsoon precipitation records of East Asia, oxygen isotopes found in Greenland ice cores, and the SST of the northern South China Sea [26,64,65]. The chemical weathering records of the BBW25 core, covering the northwest South China Sea, are predominantly influenced by the East Asian monsoon. Therefore, we anticipate conducting a comparative analysis between the chemical weathering indicators of the BBW25 core and the indicators reflecting changes in the East Asian monsoon, aiming to investigate the significant climatic events recorded by the core since the late LGM.

4.2.2. Effective Chemical Weathering Intensity

The various geochemical elements in the BBW25 core sediments were greatly affected by the marine and terrestrial environments, making it difficult to conduct a comprehensive comparison of chemical weathering intensity. Therefore, selecting climate indicators that were less affected by sedimentary environments was crucial. As shown in Figure 9, major elements such as Al, Fe, K, and Na did not show a marked “jump” at the depth of 119–120 cm. Thus, these elements were less affected by the marine and terrestrial environ-

mental conditions. Therefore, using these elements to establish weathering indicators was more effective.

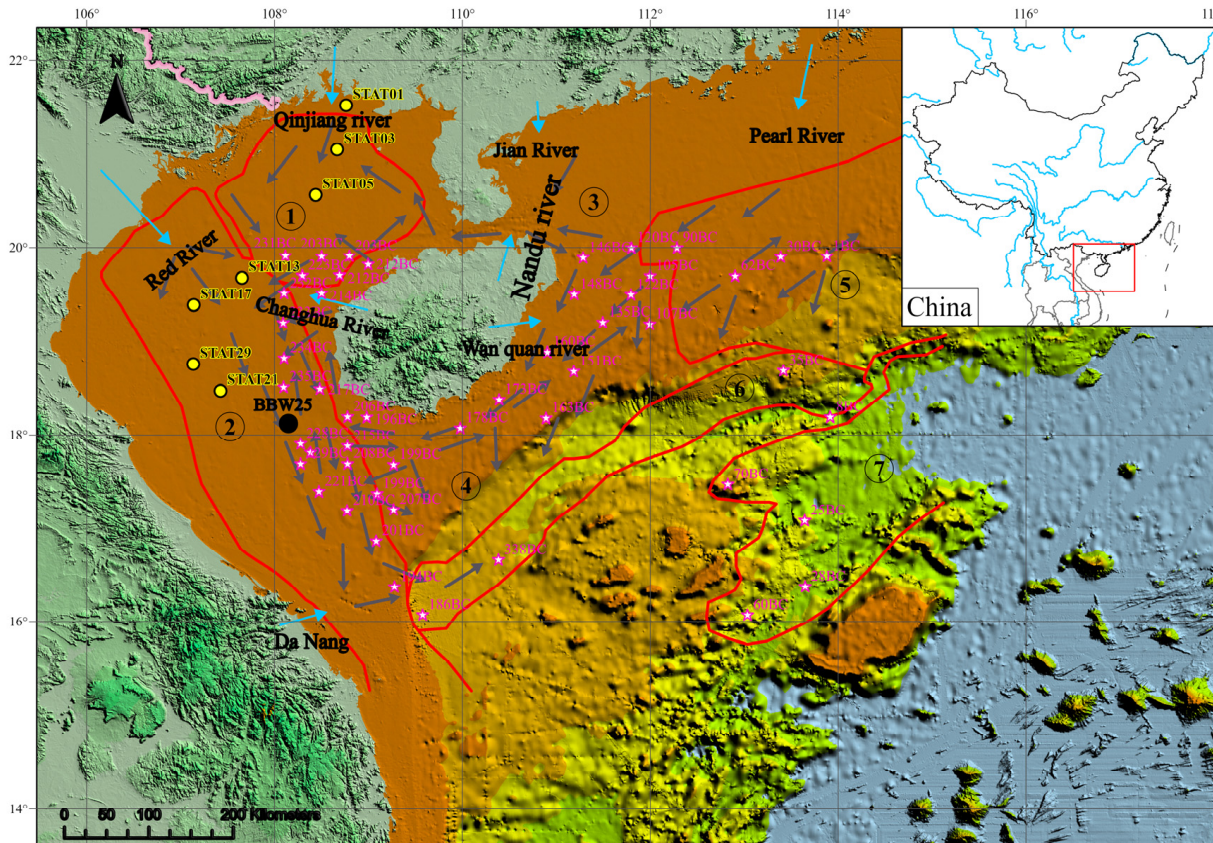


Figure 8. Source-to-sink processes in the northwestern part of South China Sea [66,67]. (1) Source: the starting point of the blue arrow is the source of terrigenous clastic sediments; (2) channel: the gray arrow direction is the main sediment transport direction and its pathway; (3) sinks: the circle number is the sedimentary block number: ① Beibu Gulf Basin; ② Yinggehai Basin; ③ shallow shelf around Hainan Island; ④ Qiongdongnan Basin; ⑤ Pearl River Estuary Basin; ⑥ Xisha Trough; ⑦ Sea Basin. (4) Black spot: BBW25 core; (5) yellow spots: STAT cores; pink stars: PC cores.

During chemical weathering, Al is a conservative and non-migratory element and remains unchanged compared to the mother rock and sediments. Na is highly mobile and readily departs from the mother rock and sediments. Therefore, Na is usually depleted in weathering products. K is easily leached from primary minerals but is resistant to leaching and is immobilized by secondary clay minerals in the weathering profiles. The modified chemical alteration index (CIX) can link the three elements ($CIX = 100 \times Al_2O_3 / (Al_2O_3 + Na_2O + K_2O)$). This index can well-eliminate the influence of carbonates and phosphates on silicates [68–72]. The Al/Fe ratio refers to the degree of aluminum removal and iron enrichment. The higher the value, the stronger the degree of weathering, indicating a humid and hot climate. On the contrary, a lower value indicates a relatively dry and cold climate [73–75]. This research chose the CIX and Al/Fe ratio as indicators of the intensity of chemical weathering in the sedimentary record in the core.

4.2.3. Response of Chemical Weathering Intensity Changes Recorded in Core to the Last Major Climate Event

Previous studies on the weathering records have indicated that the chemical weathering intensity of rocks under relatively warm and humid climates is higher than that during cold and dry periods [76–78]. When the sediment source remains stable, the rock type can serve as an indicator of weathering intensity. Kaolin is predominantly formed

in a warm and humid acidic environment through extensive leaching of feldspar, mica, and pyroxene, thus representing a highly weathered mineral. In contrast, illite forms under dry and cold climatic conditions by undergoing weathering processes that involve potassium removal. If the climate becomes humid and hot and chemical weathering is thorough, potassium is taken away, and illite will further decompose into kaolinite [26]. The temperature during the late LGM–deglaciation stage was found to be lower than that of the Holocene, as indicated by the global average surface temperature curve in Figure 6. Additionally, it was observed that the upper section of the BBW25 core exhibited lower levels of illite and potassium content compared to those of the lower section, suggesting a correlation between chemical weathering intensity and variations in cold and warm climates. The chemical weathering recorded in the BBW25 core sediments can be attributed to the northwest region of the South China Sea, which was influenced by the East Asian monsoon [26]. Simultaneously, a comparison was made between the chemical weathering indicators under the “simplified framework” and the indicators for recording East Asian monsoon changes (Figure 9) to demonstrate their reliability.

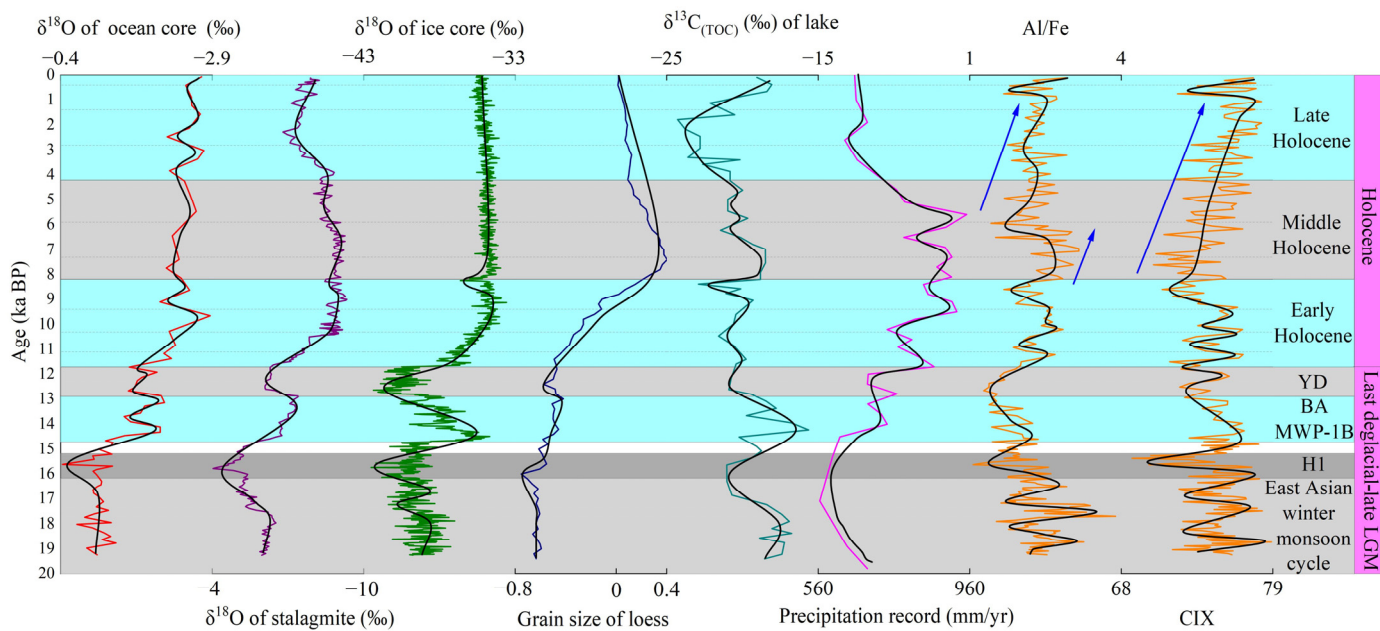


Figure 9. Comparison of age versus chemical weathering intensity curve in the core with $\delta^{18}\text{O}$ of 1144 core in South China Sea [79], $\delta^{18}\text{O}$ of stalagmites in Sanbao Cave [80], $\delta^{18}\text{O}$ of ice core in Greenland [81], grain size of loess in China [82], $\delta^{13}\text{C}(\text{TOC})$ of Lake Huguangmaer [83], and monsoon precipitation records of East Asia [84].

Based on the recorded changes in chemical weathering intensity in the core under the “simplified framework” and the analysis of major climate events since the end of the LGM (Figure 9), the BBW25 core records can be divided into the following three periods and eight climate events:

(1) Records of strong East Asian winter monsoon and weak cycles from the late LGM to the early deglaciation.

Previous studies have indicated that the South China Sea experienced a prevailing winter monsoon during the late last glacial maximum (LGM). The variations in chemical weathering intensity may serve as indicators of both intensified winter monsoon and reduced cyclical changes during this period. Consequently, the elevated terrestrial input characteristics likely reflect the substantial sea level drop and oceanic current dynamics driven by the robust winter monsoon during the late LGM [85–87].

(2) Records of alternating cold and warm climate events and meltwater events during the last deglaciation.

① The H1 cold event with cold and dry happened at high latitudes in the Northern Hemisphere, but with a slight increase in humidity in comparison to that in the late LGM [88,89]. The H1 cold event was clearly documented in the BBW25 core, with a distinct decline observed in the chemical weathering intensity indicated by the Fe/Al ratio and CIX. Simultaneously, $\delta^{18}\text{O}$ levels increased in South China Sea cores during the H1 cold event, suggesting that both the northern part of the South China Sea and southern China experienced a cold and arid climate during this period. The coarsening of particles in loess sediments, reduction in carbon isotopes within lakes, and decreased precipitation all indicate a dry and frigid climate across East Asia.

② The BA warm event happened because of the involvement of thermohaline circulation during the last deglaciation, and geological reconstruction data and numerical simulations confirmed this point. Greenland's temperature increased by about 10 °C during this event [90–95]. The $\delta^{18}\text{O}$ records of stalagmites and the South China Sea cores as well as the carbon isotope records of lacustrine sediments showed that the BA warm regions in the Northern Hemisphere. The rising trend in precipitation in East Asia at this time suggested a warm and humid climate. The enhanced chemical weathering intensity recorded in the BBW25 core during this stage was the response to the BA warm event. Meanwhile, the sedimentary environment indicator records responded well to the MWP-1A event. At this time, the significant rise in sea level led to a transition from terrestrial inputs to marine inputs. Therefore, it was believed that the low terrestrial input and high weathering intensity at this time can serve as indirect evidence for the synchronous start of the MWP-1A and BA warm events.

③ During the YD period, $\delta^{18}\text{O}$ of the Greenland ice core decreased, which indicated the cooling of high-latitude regions in the Northern Hemisphere. The SST in the South China Sea showed a decrease in temperature during the YD cold event compared to that during the BA warm event. The grain size of loess on the Loess Plateau became coarser, and $\delta^{18}\text{O}$ of stalagmites rose. The pollen records of lacustrine sediments indicated an increase in psychrophilic plants during the YD cold event [96–98]. The decrease in chemical weathering intensity recorded by BBW25 was a response to the YD cold event.

(3) Early Holocene climate oscillations and records of abrupt climate changes from the Middle to the Late Holocene.

① Previous studies have found that during the climate warming process towards the Holocene at the end of the last deglaciation, there were multiple climate oscillations in the early Holocene, manifested as transient dry and cold events; this was caused by the strongest summer monsoon event and winter monsoon strengthening event during the early Holocene ice age [15,87]. According to [14], three cooling events were found to occur at 9.4, 10.3, and 11.1 ka BP, respectively. The changes characteristics of the three cycles recorded by chemical weathering in the BBW25 core sediments from the late Younger Dryas event to early Holocene respond to the circle climate change events of the temperature decreasing and the winter monsoon strengthening during the ice age, while the temperature increasing and the summer monsoon strengthening during the interglacial period within a century scale of the early Holocene [99].

② There were several climate events from the Middle to the Late Holocene, among which the 8.2 ka BP event, as the beginning of the Middle Holocene, was possibly the strongest cold event since the Holocene; changes in the monsoon precipitation in the Northern Hemisphere were mainly caused by freshwater injection [100,101]. Figure 9 shows that the intensity of weathering recorded in the core had a significant decrease from 8.8 to 8 ka BP. After 8 ka BP, chemical weathering intensified, indicating the onset of a warm and humid climate.

③ A decline in chemical weathering recorded by the Al/Fe ratio from 7 ka BP to 5 ka BP may be related to the 5.9 ka BP event, which was a sudden cold climate change that occurred in the Middle Holocene; during this period, the dormant ENSO climate became active again [102,103]. This cold event has been recorded in lake sediments, loess sediments, ice core, and the change in sea level in China [104–106].

④ The most recent decline in chemical weathering in the core from modern times may have been caused by the Little Ice Age, with typical time of 0.4 ka BP and record age range of 0.6–0.15 ka BP in China [15,107]. The sedimentary data suggest that the Little Ice Age may have been the most severe cold event in the past three millennia. Glacier and lake records in the middle and high latitudes of the Northern Hemisphere indicate a cold climate, while stalagmite records in the low latitudes of the Northern Hemisphere suggest an arid climate [108–111].

The average values of CIX and Fe/Al ratio in the Holocene and the late LGM-deglaciation stage were 74.88 and 2.44, respectively, and 74.84 and 2.27, indicating that the chemical weathering intensity recorded in the study area during the Holocene was slightly higher than that during the late LGM—deglaciation stage.

5. Conclusions

According to the profile variation in the content of major and trace elements, TOC and TN, CaCO_3 , and the value of $\delta^{13}\text{C}$ on the P36 core sediments combined with AMS 14C dating, the following points could be concluded:

(1) The BBW25 sediment core was deposited from the late Pleistocene. And taking the depth of 119 cm as the boundary, the BBW25 core could be divided into two sedimentary sections based on the change of geochemical characteristics: the low section and the upper section. The upper section is the depth of 0 to 119 cm which sedimentary ages are from present day to 14.54 ka BP. And the low section is the depth of 119 to 210 cm, whose sedimentary ages are from 14.54 to 19.24 ka BP. The reason for this phenomenon is due to a sedimentary environment change from terrestrial to marine environments.

(2) According to sedimentary environment indicators, the Beibu Gulf is divided into three sedimentary environments (terrestrial, marine–terrestrial alternating, and marine) and five sedimentary sub-environments (paleo-bay, transgression regression, transgression, paleo-bay, and modern gulf). By analyzing the sedimentary indicators in this study and previous research on other cores in the Beibu Gulf. The division of sedimentary environments in the Beibu Gulf obtained was more similar to the results obtained by previous researchers through a comprehensive analysis of C4 and B106 cores. This also indicated that the extracted Sr/Ba value was more accurate in dividing sedimentary environments than the total Sr/Ba value.

(3) The major climate events recorded by the CIX and the Al/Fe ratio in the BBW25 core since the late LGM include the East Asian winter monsoon cycle in the late LGM, the H1 cold event, the BA warm event, the MWP-1A event, the YD cold event, the 8.2 ka B.P. cold event, the 5.9 ka B.P. cold event, and the Little Ice Age event; the chemical weathering intensity recorded in the Holocene is slightly greater than that of the late LGM—deglaciation stage.

(4) In summary, the comparison of the sedimentary environments and chemical weathering intensity changes in BBW25 core sedimentary records with major climate events since the end of the LGM can help to prove the reliability of the simplified framework established in this paper. It can fully contribute to a better understanding of marine paleoenvironmental change in the Beibu Gulf and regional response of the marginal seas over to the sea level of South China Sea changes and the northern Hemisphere climate reconstruction since the late LGM, and which can be used as a reference for the future climate change research.

Author Contributions: Conceptualization, T.F.; methodology, Y.L. (Yuchun Li); software, Y.L. (Yuchun Li); validation, Y.L. (Yuchun Li); formal analysis, Y.L. (Yuchun Li); data curation, Y.L. (Yuchun Li) and T.F.; writing—original draft preparation, Y.L. (Yuchun Li); review and editing, Y.L. (Yuchun Li) and T.F.; providing partial experimental methods, A.W.; test funding support, J.Z. and Y.L. (Yubiao Lv); partial experimental work, M.Z. and D.L. Data and samples were collected from the open research cruise (number: NORC2021-11) supported by NSFC Shiptime Sharing Project 2020. All authors have read and agreed to the published version of the manuscript.

Funding: This research was funded by the Science Fund Project of Fangchenggang (2022BB141154, AB22013011).

Institutional Review Board Statement: Not applicable.

Informed Consent Statement: Not applicable.

Data Availability Statement: The data presented in this study are available on request from the first author or the corresponding author.

Acknowledgments: We thank Yue, Y.F., Wei L. and Zhang N.N. for their recommendations. We thank the anonymous reviewers for their comments and suggestions, which greatly improved the manuscript.

Conflicts of Interest: The authors declare no conflicts of interest.

References

- Huang, J.; Jiang, F.; Wan, S.; Zhang, J.; Li, A.; Li, T. Terrigenous supplies variability over the past 22,000 yr in the southern South China Sea slope: Relation to sea level and monsoon rainfall changes. *J. Asian Earth Sci.* **2016**, *117*, 317–327. [[CrossRef](#)]
- Li, M.; Ouyang, T.; Tian, C.; Zhu, Z.; Peng, S.; Tang, Z.; Qiu, Y.; Zhong, H.; Peng, X. Sedimentary responses to the East Asian monsoon and sea level variations recorded in the northern South China Sea over the past 36 kyr. *J. Asian Earth Sci.* **2019**, *171*, 213–224. [[CrossRef](#)]
- Liu, Z.; Zhao, Y.; Colin, C.; Stattegger, K.; Wiesner, M.G.; Huh, C.A.; Zhang, Y.; Li, X.; Sompongchaiyakul, P.; You, C.F.; et al. Source-to-sink transport processes of fluvial sediments in the South China Sea. *Earth Sci. Rev.* **2016**, *153*, 238–273. [[CrossRef](#)]
- Liu, F.; Yang, C.; Chang, X.; Liao, Z. Provenance discrimination of the last glacial sediments from the northeastern South China Sea and its paleoenvironmental indications. *Terr. Atmos. Ocean. Sci.* **2018**, *29*, 131–148. [[CrossRef](#)]
- Hanebuth, T.; Stattegger, K.; Grootes, P.M. Rapid flooding of the Sunda Shelf: A late-glacial sea-level record. *Science* **2000**, *288*, 1033–1035. [[CrossRef](#)] [[PubMed](#)]
- Yokoyama, Y.; Lambeck, K.; De Deckker, P.; Johnston, P.; Fifield, K.L. Timing of the Last Glacial Maximum from observed sea-level minima. *Nature* **2000**, *406*, 713–716. [[CrossRef](#)]
- Rohling, E.J.; Grant, K.; Bolshaw, M.; Roberts, A.P.; Siddall, M.; Hemleben, C.; Kucera, M. Antarctic temperature and global sea level closely coupled over the past five glacial cycles. *Nat. Geosci.* **2009**, *2*, 500–504. [[CrossRef](#)]
- Pelejero, C.; Grimalt, J.O. The correlation between the ^{37}K index and sea surface temperatures in the warm boundary: The South China Sea. *Geochim. Cosmochim. Acta* **1997**, *61*, 4789–4797. [[CrossRef](#)]
- Pelejero, C.; Grimalt, J.O.; Heilig, S.; Kienast, M.; Wang, L. High-resolution ^{37}K temperature reconstructions in the South China Sea over the past 220 kyr. *Paleoceanography* **1999**, *14*, 224–231. [[CrossRef](#)]
- Xia, P.; Meng, X.; Li, Z.; Zhi, P.; Zhao, M.; Wang, E. Late Holocene mangrove development and response to sea level change in the northwestern South China Sea. *Acta Oceanol. Sin.* **2019**, *38*, 111–120. [[CrossRef](#)]
- Zhou, G.; Cao, X.; Xia, J.; Wang, S.; Song, Z. A Dramatic Marine Environment Change in the Beibu Gulf of the South China Sea around 3.2 kyr BP. *Lithosphere* **2022**, *2022*, 2632112. [[CrossRef](#)]
- Wang, J.Y.; Bai, W.M.; Wang, Z.B.; Wang, M.H.; Li, B.J. Holocene climate evolution in eastern China and its correspondence with climate events. *Mar. Geol. Quat. Geol.* **2022**, *2*, 167–177.
- Bond, G.; Kromer, B.; Beer, J.; Muscheler, R.; Evans, M.N.; Showers, W.; Hoffmann, S.; Lotti-Bond, R.; Hajdas, I.; Bonani, G. Persistent solar influence on North Atlantic climate during the Holocene. *Science* **2001**, *294*, 2130–2136. [[CrossRef](#)] [[PubMed](#)]
- Bond, G.; Showers, W.; Cheseby, M.; Lotti, R.; Almasi, P.; DeMenocal, P.; Priore, P.; Cullen, H.; Hajdas, I.; Bonani, G. A pervasive millennial-scale cycle in North Atlantic Holocene and glacial climates. *Science* **1997**, *278*, 1257–1266. [[CrossRef](#)]
- Wang, S.W. Holocene cold events in the North Atlantic: Chronology and climate impact. *Quat. Res.* **2009**, *29*, 1146–1153.
- Li, X.; Liu, X.; Pan, Z.; Shi, Z.; Xie, X.; Ma, H.; Zhai, J.; Liu, H.; Xie, X.; Dai, A. Transient vegetation degradation reinforced rapid climate change (RCC) events during the Holocene. *npj Clim. Atmos. Sci.* **2023**, *6*, 125. [[CrossRef](#)]
- Li, X.; Liu, X.; Pan, Z.; Xie, X.; Shi, Z.; Wang, Z.; Bai, A. Orbital-scale dynamic vegetation feedback caused the Holocene precipitation decline in northern China. *Commun. Earth Environ.* **2022**, *3*, 257. [[CrossRef](#)]
- Zhou, S.Z.; Zhao, J.D.; Wang, J.; Xu, L.B.; Cui, J.X.; Ou, X.J.; Xie, J.M. Quaternary cryosphere-Long-scale study of global change. *J. China Acad. Sci.* **2020**, *4*, 475–483. [[CrossRef](#)]
- Wu, K.; Shi, X.; Lou, Z.; Wu, B.; Li, J.; Zhang, H.; Cao, P.; Rahim Mohamed, C.A. Sedimentary responses to climate changes and human activities over the past 7400 Years in the western sunda shelf. *Front. Earth Sci.* **2021**, *9*, 631815. [[CrossRef](#)]
- Sun, X.; Li, X.; Beug, H.J. Pollen distribution in hemipelagic surface sediments of the South China Sea and its relation to modern vegetation distribution. *Mar. Geol.* **1999**, *156*, 211–226. [[CrossRef](#)]
- Li, Z.; Zhang, Y.; Li, Y.; Zhao, J. Palynological records of Holocene monsoon change from the Gulf of Tonkin (Beibuwan), northwestern South China Sea. *Quat. Res.* **2010**, *74*, 8–14. [[CrossRef](#)]
- Huang, X.Q.; Liang, K.; Xi, L.; Xia, Z.; Zhang, S.Z. Holocene transgression evolution in Beibu Gulf and its relationship with climate and glaciers. *Acta Geologica Sinica* **2022**, *1*, 49–64.
- Cui, Z.; Schulz-Bull, D.E.; Hou, Y.; Xia, Z.; Waniek, J.J. Geochemical characteristics and provenance of Holocene sediments (core STAT22) in the Beibu Gulf, South China Sea. *J. Coast. Res.* **2016**, *32*, 1105–1115. [[CrossRef](#)]

24. Li, M.; Ouyang, T.; Roberts, A.P.; Heslop, D.; Zhu, Z.; Zhao, X.; Tian, C.; Peng, S.; Zhong, H.; Peng, X.; et al. Influence of sea level change and centennial East Asian monsoon variations on northern South China Sea sediments over the past 36 kyr. *Geochem. Geophys. Geosyst.* **2018**, *19*, 1674–1689. [[CrossRef](#)]
25. Zhao, Z.X.; Wan, S.M.; Ju, M.S.; Pei, W.Q.; Jin, H.L.; Zhang, J.; Li, A.C. Sr-Nd isotope and rare earth element evidence of sediment sources and weathering evolution in the northwest of the South China Sea since the last glacial period. *Bull. Miner. Rock Geochem.* **2023**, *4*, 702–716+682–683. [[CrossRef](#)]
26. Wan, S.M.; Qin, L.; Yang, S.Y.; Zhao, D.B.; Zhang, J.; Jiao, D.F.; Li, T.G. Glacial shelf weathering and carbon cycle in the South China Sea. *Quat. Study* **2020**, *6*, 1532–1549.
27. GB/T 14506.31-2019; Chemical Analysis Methods of Silicate Rocks Part 31: Determination of 12 Components Such as Silica—Lithium Metaborate Melting-Inductively Coupled Plasma Atomic Emission Spectrometry. National Technical Committee for Standardization of Land and Resources: Geneva, Switzerland, 2019.
28. GB/T 14506.30-2010; Chemical Analysis Methods of Silicate Rocks Part 30: Determination of 44 Elements. National Technical Committee for Standardization of Land and Resources: Geneva, Switzerland, 2010.
29. Wang, A.H.; Ye, S.Y.; Liu, J.K.; Ding, X.G.; Li, H.L.; Xu, N.C. Discussion on the discrimination of marine sedimentary environment with different selective extraction methods of strontium and barium ratio—Taking the modern Yellow River Delta as an example. *Acta Sedimentol.* **2020**, *6*, 1226–1238. [[CrossRef](#)]
30. Blaauw, M.; Christen, J.A. Flexible paleoclimate age-depth models using an autoregressive gamma process. *Bayesian Anal.* **2011**, *6*, 457–474. [[CrossRef](#)]
31. Tanabe, S.; Hori, K.; Saito, Y.; Haruyama, S.; Kitamura, A. Song Hong (Red River) delta evolution related to millennium-scale Holocene sea-level changes. *Quat. Sci. Rev.* **2003**, *22*, 2345–2361. [[CrossRef](#)]
32. Armstrong-Altrin, J.S.; Machain-Castillo, M.L.; Rosales-Hoz, L.; Carranza-Edwards, A.; Sanchez-Cabeza, J.A.; Ruíz-Fernández, A.C. Provenance and depositional history of continental slope sediments in the Southwestern Gulf of Mexico unraveled by geochemical analysis. *Cont. Shelf Res.* **2015**, *95*, 15–26. [[CrossRef](#)]
33. Liu, Y.J. *Element Geochemistry*; Science Press: Beijing, China, 1984.
34. Wang, A.; Wang, Z.; Liu, J.; Xu, N.; Li, H. The Sr/Ba ratio response to salinity in clastic sediments of the Yangtze River Delta. *Chem. Geol.* **2021**, *559*, 119923. [[CrossRef](#)]
35. Dashtgard, S.E.; Wang, A.; Pospelova, V.; Wang, P.L.; La Croix, A.; Ayrancı, K. Salinity indicators in sediment through the fluvial-to-marine transition (Fraser River, Canada). *Sci. Rep.* **2022**, *12*, 14303. [[CrossRef](#)] [[PubMed](#)]
36. Meyers, P.A. Preservation of elemental and isotopic source identification of sedimentary organic matter. *Chem. Geol.* **1994**, *114*, 289–302. [[CrossRef](#)]
37. Lamb, A.L.; Wilson, G.P.; Leng, M.J. A review of coastal palaeoclimate and relative sea-level reconstructions using $\delta^{13}\text{C}$ and C/N ratios in organic material. *Earth Sci. Rev.* **2006**, *75*, 29–57. [[CrossRef](#)]
38. Thornton, S.F.; McManus, J. Application of organic carbon and nitrogen stable isotope and C/N ratios as source indicators of organic matter provenance in estuarine systems: Evidence from the Tay Estuary, Scotland. *Estuar. Coast. Shelf Sci.* **1994**, *38*, 219–233. [[CrossRef](#)]
39. Milliman, J.D.; Qinchun, X.; Zuosheng, Y. Transfer of particulate organic carbon and nitrogen from the Yangtze River to the ocean. *Am. J. Sci.* **1984**, *284*, 824–834. [[CrossRef](#)]
40. Middelburg, J.J.; Nieuwenhuize, J. Carbon and nitrogen stable isotopes in suspended matter and sediments from the Schelde Estuary. *Mar. Chem.* **1998**, *60*, 217–225. [[CrossRef](#)]
41. Chmura, G.L.; Aharon, P. Stable carbon isotope signatures of sedimentary carbon in coastal wetlands as indicators of salinity regime. *J. Coast. Res.* **1995**, *11*, 124–135. Available online: <http://www.jstor.org/stable/4298316> (accessed on 1 October 2023).
42. Khan, N.S.; Vane, C.H.; Horton, B.P. Stable carbon isotope and C/N geochemistry of coastal wetland sediments as a sea-level indicator. *Handb. Sea-Level Res.* **2015**, 295–311. [[CrossRef](#)]
43. Zhang, N. *The Mineralogical Characteristics of the Sediments and Its Environmental Significance in the Beibuwan Gulf*; China University of Geosciences: Beijing, China, 2015.
44. Ni, Y.G.Y.; Xia, Z.; Ma, S.Z. The opening of Qiongzhou Strait: Evidence from sub-bottom profiles. *Mar. Geol. Quat. Geol.* **2014**, *34*, 79–82.
45. Li, C.R.; Yang, X.; Fan, C.; Hu, L.; Dai, L.; Zhao, S. On the Evolution Process of the Beibu Gulf Basin and Forming Mechanism of Local Structures. *Acta Geol. Sin.* **2018**, *92*, 2028–2039. [[CrossRef](#)]
46. Kaboth-Bahr, S.; Bahr, A.; Yamoah, K.A.; Chuang, C.K.; Li, H.C.; Su, C.C.; Wei, K.Y. Rapid humidity changes across the Northern South China Sea during the last ~40 kyrs. *Mar. Geol.* **2021**, *440*, 106579. [[CrossRef](#)]
47. Snyder, C.W. Evolution of global temperature over the past two million years. *Nature* **2016**, *538*, 226–228. [[CrossRef](#)] [[PubMed](#)]
48. Wan, S.; Clift, P.D.; Zhao, D.; Hovius, N.; Munhoven, G.; France-Lanord, C.; Wang, Y.; Xiong, Z.; Huang, J.; Yu, Z.; et al. Enhanced silicate weathering of tropical shelf sediments exposed during glacial lowstands: A sink for atmospheric CO₂. *Geochim. Cosmochim. Acta* **2017**, *200*, 123–144. [[CrossRef](#)]
49. Cang, S.C.; Chen, L.R.; Dong, T.L. Study on evolution history of sedimentary environment since Pliocene in R_1 core of Beibu Gulf. *Mar. Geol. Quat. Geol.* **1992**, *4*, 53–58. [[CrossRef](#)]
50. Xu, D. *Sedimentary Records Since the Last Deglaciation Period in the Eastern Beibu Gulf and the Formation of Modern Sedimentary Pattern*; Graduate School of China Academy of Sciences (Institute of Oceanography): Beijing, China, 2014.

51. Zhang, L.L.; Chen, M.H.; Chen, Z.; Xiang, R.; Liu, J.G. Distribution of calcium carbonate content in surface sediments of the South China Sea and its influencing factors. *Geosci. J. China Geo Univ.* **2010**, *6*, 891–898.
52. Huang, E.Q.; Tian, J. Melting water events and abrupt climate change in the last deglaciation period. *Sci. Bull.* **2008**, *12*, 1437–1447.
53. Zhao, H.T. Origin and time of Qiongzhou Strait. *Mar. Geol. Quat. Geol.* **2007**, *27*, 33–40.
54. Yao, Y.; Harff, J.; Meyer, M.; Zhan, W. Reconstruction of paleocoastlines for the northwestern South China Sea since the Last Glacial Maximum. *Sci. China Ser. D Earth Sci.* **2009**, *52*, 1127–1136. [[CrossRef](#)]
55. Dykoski, C.A.; Edwards, R.L.; Cheng, H.; Yuan, D.; Cai, Y.; Zhang, M.; Lin, Y.; Qing, J.; An, Z.; Revenaugh, J. A high-resolution, absolute-dated Holocene and deglacial Asian monsoon record from Dongge Cave, China. *Earth Planet. Sci. Lett.* **2005**, *233*, 71–86. [[CrossRef](#)]
56. Huang, J.; Li, A.; Wan, S. Sensitive grain-size records of Holocene East Asian summer monsoon in sediments of northern South China Sea slope. *Quat. Res.* **2011**, *75*, 734–744. [[CrossRef](#)]
57. Wang, L.; Li, J.; Lu, H.; Gu, Z.; Rioual, P.; Hao, Q.; Mackay, A.W.; Jiang, W.; Cai, B.; Xu, B.; et al. The East Asian winter monsoon over the last 15,000 years: Its links to high-latitudes and tropical climate systems and complex correlation to the summer monsoon. *Quat. Sci. Rev.* **2012**, *32*, 131–142. [[CrossRef](#)]
58. Wang, P.X. *Collected Papers on Marine Microorganisms and Paleontology*; Ocean Press: Beijing, China, 1980.
59. Li, G.Z.; Bian, Y.H.; Wang, P.X. Holocene transgressive strata and their microfossil characteristics in the northeast of Beibu Gulf. *Trop. Ocean* **1988**, *2*, 63–70.
60. Yang, S.; Li, C.; Cai, J. Geochemical compositions of core sediments in eastern China: Implication for Late Cenozoic palaeoenvironmental changes. *Palaeogeogr. Palaeoclimatol. Palaeoecol.* **2006**, *229*, 287–302. [[CrossRef](#)]
61. Wei, G.; Liu, Y.; Li, X.; Shao, L.; Liang, X. Climatic impact on Al, K, Sc and Ti in marine sediments: Evidence from ODP Site 1144, South China Sea. *Geochem. J.* **2003**, *37*, 593–602. [[CrossRef](#)]
62. Wei, G.; Liu, Y.; Li, X.; Chen, M.; Wei, W. High-resolution elemental records from the South China Sea and their paleoproductivity implications. *Paleoceanography* **2003**, *18*, 1054. [[CrossRef](#)]
63. Murray, R.W.; Knowlton, C.; Leinen, M.; Mix, A.C.; Polksy, C.H. Export production and terrigenous matter in the Central Equatorial Pacific Ocean during interglacial oxygen isotope Stage 11. *Glob. Planet. Chang.* **2000**, *24*, 59–78. [[CrossRef](#)]
64. Wan, S.; Toucanne, S.; Clift, P.D.; Zhao, D.; Bayon, G.; Yu, Z.; Cai, G.; Yin, X.; Révillon, S.; Wang, D.; et al. Human impact overwhelms long-term climate control of weathering and erosion in southwest China. *Geology* **2015**, *43*, 439–442. [[CrossRef](#)]
65. Hu, D.; Clift, P.D.; Böning, P.; Hannigan, R.; Hillier, S.; Blusztajn, J.; Wan, S.; Fuller, D.Q. Holocene evolution in weathering and erosion patterns in the Pearl River delta. *Geochem. Geophys. Geosyst.* **2013**, *14*, 2349–2368. [[CrossRef](#)]
66. Qiu, Y.; Peng, X.C.; Wang, Y.M.; Huang, W.K.; Du, W.B. *Quaternary Erosion Process and Sedimentary Response in the Northern South China Sea*; Geology Press: Beijing, China, 2017.
67. Li, M.K. *Evolution and Driving Mechanism of Paleoclimate and Environment since 36 Kyr BP in the Northwest South China Sea*; University of Chinese Academy of Sciences (Guangzhou Institute of Geochemistry, China Academy of Sciences): Beijing, China, 2018.
68. Nesbitt, H.W.; Markovics, G. Weathering of granodioritic crust, long-term storage of elements in weathering profiles, and petrogenesis of siliciclastic sediments. *Geochim. Cosmochim. Acta* **1997**, *61*, 1653–1670. [[CrossRef](#)]
69. Li, X.H.; Wei, G.; Shao, L.; Liu, Y.; Liang, X.; Jian, Z.; Sun, M.; Wang, P. Geochemical and Nd isotopic variations in sediments of the South China Sea: A response to Cenozoic tectonism in SE Asia. *Earth Planet. Sci. Lett.* **2003**, *211*, 207–220. [[CrossRef](#)]
70. Yang, S.; Jung, H.S.; Li, C. Two unique weathering regimes in the Changjiang and Huanghe drainage basins: Geochemical evidence from river sediments. *Sediment. Geol.* **2004**, *164*, 19–34. [[CrossRef](#)]
71. Wei, G.; Li, X.H.; Liu, Y.; Shao, L.; Liang, X. Geochemical record of chemical weathering and monsoon climate change since the early Miocene in the South China Sea. *Paleoceanography* **2006**, *21*, PA4214. [[CrossRef](#)]
72. Garzanti, E.; Padoan, M.; Setti, M.; López-Galindo, A.; Villa, I.M. Provenance versus weathering control on the composition of tropical river mud (southern Africa). *Chem. Geol.* **2014**, *366*, 61–74. [[CrossRef](#)]
73. Wei, G.; Liu, Y.; Li, X.H.; Shao, L.; Fang, D. Major and trace element variations of the sediments at ODP Site 1144, South China Sea, during the last 230 ka and their paleoclimate implications. *Palaeogeogr. Palaeoclimatol. Palaeoecol.* **2004**, *212*, 331–342. [[CrossRef](#)]
74. Wang, X. *Particle Size Characteristics and Geochemical Analysis of Surface Sediment on the Seabed of Panjin Port*; Liaoning Normal University: Dalian, China, 2018.
75. Kronberg, B.I.; Nesbitt, H.W.; Lam, W.W. Upper Pleistocene Amazon deep-sea fan muds reflect intense chemical weathering of their mountainous source lands. *Chem. Geol.* **1986**, *54*, 283–294. [[CrossRef](#)]
76. West, A.J. Thickness of the chemical weathering zone and implications for erosional and climatic drivers of weathering and for carbon-cycle feedbacks. *Geology* **2012**, *40*, 811–814. [[CrossRef](#)]
77. Catalan, J.; Pla-Rabés, S.; García, J.; Camarero, L. Air temperature-driven CO₂ consumption by rock weathering at short timescales: Evidence from a Holocene lake sediment record. *Geochim. Cosmochim. Acta* **2014**, *136*, 67–79. [[CrossRef](#)]
78. West, A.J.; Galy, A.; Bickle, M. Tectonic and climatic controls on silicate weathering. *Earth Planet. Sci. Lett.* **2005**, *235*, 211–228. [[CrossRef](#)]
79. Bühring, C.; Sarnthein, M.; Erlenkeuser, H. Toward a high-resolution stable isotope stratigraphy of the last 1.1 m.y.: Site 1144, South China Sea. *Proc. ODP Sci. Results* **2014**, *184*, 1–29. [[CrossRef](#)]
80. Wang, Y.; Cheng, H.; Edwards, R.L.; Kong, X.; Shao, X.; Chen, S.; An, Z. Millennial-and orbital-scale changes in the East Asian monsoon over the past 224,000 years. *Nature* **2008**, *451*, 1090–1093. [[CrossRef](#)]

81. North Greenland Ice Core Project Members. High-resolution record of Northern Hemisphere climate extending into the last interglacial period. *Nature* **2004**, *431*, 147–151. [CrossRef] [PubMed]
82. Yang, S.; Ding, Z. A 249 kyr stack of eight loess grain size records from northern China documenting millennial-scale climate variability. *Geochem. Geophys. Geosyst.* **2014**, *15*, 798–814. [CrossRef]
83. National Earth System Science Data Sharing Service Platform. *China Sci. Technol. Resour. Guide* **2017**, *49*, 112. Available online: <https://www.geodata.cn/> (accessed on 1 October 2023).
84. Beck, J.W.; Zhou, W.; Li, C.; Wu, Z.; White, L.; Xian, F.; Kong, X.; An, Z. A 550,000-year record of East Asian monsoon rainfall from ^{10}Be in loess. *Science* **2018**, *360*, 877–881. [CrossRef] [PubMed]
85. Huang, C.Y.; Liew, P.M.; Zhao, M.; Chang, T.C.; Kuo, C.M.; Chen, M.T.; Wang, C.H.; Zheng, L.F. Deep sea and lake records of the Southeast Asian paleomonsoons for the last 25 thousand years. *Earth Planet. Sci. Lett.* **1997**, *146*, 59–72. [CrossRef]
86. Wang, L.; Sarnthein, M.; Erlenkeuser, H.; Grimalt, J.; Grootes, P.; Heilig, S.; Ivanova, E.; Kienast, M.; Pelejero, C.; Pflaumann, U. East Asian monsoon climate during the Late Pleistocene: High-resolution sediment records from the South China Sea. *Mar. Geol.* **1999**, *156*, 245–284. [CrossRef]
87. Mao, S.Y.; Zhu, X.W.; Wu, N.Y.; Sun, Y.G.; Guan, H.X. Records of Ice Melting Water and Climate Events Since the Last Glacial Maximum in the Northern South China Sea: Indications of Long Chain Fatty Alcohol Terrestrial Input. *J. Trop. Oceanogr.* **2015**, *2*, 52–65.
88. Li, M.K.; Ouyang, T.P.; Zhu, Z.Y.; Tian, C.J.; Peng, S.S.; Qiu, Y.; Peng, X.C.; Zhong, H.X.; Chen, H.J. Magnetic records of the H1 event on the northwest slope of the South China Sea. *Quat. Stud.* **2019**, *39*, 927–937. [CrossRef]
89. Yang, S.L.; Dong, X.X.; Xiao, J.L. History of East Asian Monsoon Changes Since the Last Glacial Maximum—Geological Records of Northern China. *Chin. Sci. Earth Sci.* **2019**, *49*, 1169–1181.
90. Cheng, J. *Research on the Phenomenon of “Overshoot” of Temperature and Salinity Circulation during Bølling-Allerød Warming Events*; Nanjing University of Information Science and Technology: Nanjing, China, 2013.
91. Petit, J.R.; Jouzel, J.; Raynaud, D.; Barkov, N.I.; Barnola, J.M.; Basile, I.; Bender, M.; Chappellaz, J.; Davis, M.; Delaygue, G.; et al. Climate and atmospheric history of the past 420,000 years from the Vostok ice core, Antarctica. *Nature* **1999**, *399*, 429–436. [CrossRef]
92. Cuffey, K.M.; Clow, G.D. Temperature, accumulation, and ice sheet elevation in central Greenland through the last deglacial transition. *J. Geophys. Res. Ocean.* **1997**, *102*, 26383–26396. [CrossRef]
93. Alley, R.B. Ice-core evidence of abrupt climate changes. *Proc. Natl. Acad. Sci. USA* **2000**, *97*, 1331–1334. [CrossRef] [PubMed]
94. McManus, J.F.; Francois, R.; Gherardi, J.M.; Keigwin, L.D.; Brown-Leger, S. Collapse and rapid resumption of Atlantic meridional circulation linked to deglacial climate changes. *Nature* **2004**, *428*, 834–837. [CrossRef] [PubMed]
95. Liu, Z.; Otto-Bliesner, B.L.; He, F.; Brady, E.C.; Tomas, R.; Clark, P.U.; Carlson, A.E.; Lynch-Stieglitz, J.; Curry, W.; Brook, E.; et al. Transient Simulation of Last Deglaciation with a New Mechanism for Bølling-Allerød Warming. *Science* **2009**, *325*, 310–314. [CrossRef] [PubMed]
96. Chen, F.; Xu, Q.; Chen, J.; Birks, H.J.B.; Liu, J.; Zhang, S.; Jin, L.; An, C.; Telford, R.J.; Cao, X.; et al. East Asian summer monsoon precipitation variability since the last deglaciation. *Sci. Rep.* **2015**, *5*, 11186. [CrossRef] [PubMed]
97. Ji, M.; Shen, J.; Wu, J.; Wang, Y. Paleovegetation and paleoclimate evolution of past 27.7 cal ka BP recorded by pollen and charcoal of lake Xingkai, Northeastern China. In *Earth Surface Processes and Environmental Changes in East Asia*; Kashiwaya, K., Shen, J., Kim, J., Eds.; Springer: Tokyo, Japan, 2015; pp. 81–94. [CrossRef]
98. Wu, J.; Liu, Q.; Wang, L.; Chu, G.Q.; Liu, J.Q. Vegetation and climate change during the last deglaciation in the Great Khingan Mountain, Northeastern China. *PLoS ONE* **2016**, *11*, e0146261. [CrossRef] [PubMed]
99. Wang, B.Y. *Research on the Instability and Suitable Period of the Early Holocene Monsoon Climate Recorded by Chinese Stalagnites*; Southwest University: Chongqing, China, 2019.
100. O’Brien, S.R.; Mayewski, P.A.; Meeker, L.D.; Meese, D.A.; Twickler, M.S.; Whitlow, S.I. Complexity of Holocene climate as reconstructed from a Greenland ice core. *Science* **1995**, *270*, 1962–1964. [CrossRef]
101. Zhang, H.L.; Pu, X.Q. Stalagmite records of climate evolution and cold dry events in the Xundian area of Yunnan during the Middle Holocene. *J. Earth Sci.* **2011**, *32*, 95–100. [CrossRef]
102. Sandweiss, D.H.; Maasch, K.A.; Anderson, D.G. Transitions in the mid-Holocene. *Science* **1999**, *283*, 499–500. [CrossRef]
103. Spindler, K. *The Man in the Ice: The Discovery of a 5000-Year-Old Body Reveals the Secrets of the Stone Age*; Harmony Books: New York, NY, USA, 1994.
104. Zhang, Z.K.; Wang, S.M.; Wu, R.J. Environmental Evolution and Southwest Monsoon Changes of Sedimentary Records of Erhai Lake in the Middle Holocene. *Sci. Bull.* **1998**, *19*, 2127–2128.
105. Yang, H.R.; Xie, Z.R. Climate fluctuations and sea level fluctuations in eastern China over the past 20000 years. *Ocean Lakes* **1984**, *1*, 1–13.
106. Huang, C.C.; Zhou, J.; Pang, J.; Han, Y.; Hou, C. A regional aridity phase and its possible cultural impact during the Holocene Megathermal in the Guanzhong Basin, China. *Holocene* **2000**, *10*, 135–142. [CrossRef]
107. Zhu, K.Z. Preliminary Study on Climate Change in China over the Past 5000 Years. *Meteorolog. Sci. Technol. Data* **1973**, *S1*, 2–23. [CrossRef]
108. Moros, M.; Andrews, J.T.; Eberl, D.D.; Jansen, E. Holocene history of drift ice in the northern North Atlantic: Evidence for different spatial and temporal modes. *Paleoceanography* **2006**, *21*, PA2017. [CrossRef]

109. Bond, G.C.; Showers, W.; Elliot, M.; Evans, M.; Lotti, R.; Hajdas, I.; Johnson, S. The North Atlantic's 1–2 kyr climate rhythm: Relation to Heinrich events, Dansgaard/Oeschger cycles and the Little Ice Age. *Geophys. Monogr. Am. Geophys. Union* **1999**, *112*, 35–58. [[CrossRef](#)]
110. Holzhauser, H.; Magny, M.; Zumbühl, H.J. Glacier and lake-level variations in west-central Europe over the last 3500 years. *Holocene* **2005**, *15*, 789–801. [[CrossRef](#)]
111. Wang, Y.; Cheng, H.; Edwards, R.L.; He, Y.; Kong, X.; An, Z.; Wu, J.; Kelly, M.J.; Dykoski, C.A.; Li, X. The Holocene Asian monsoon: Links to solar changes and North Atlantic climate. *Science* **2005**, *308*, 854–857. [[CrossRef](#)]

Disclaimer/Publisher's Note: The statements, opinions and data contained in all publications are solely those of the individual author(s) and contributor(s) and not of MDPI and/or the editor(s). MDPI and/or the editor(s) disclaim responsibility for any injury to people or property resulting from any ideas, methods, instructions or products referred to in the content.